

This is an Open Access document downloaded from ORCA, Cardiff University's institutional repository: <https://orca.cardiff.ac.uk/id/eprint/167671/>

This is the author's version of a work that was submitted to / accepted for publication.

Citation for final published version:

Murowchick, J.B., Oldroyd, A. and Rickard, D. 2024. Molecular mechanism of the sulfide corrosion of α -iron. *Corrosion Science* 231 , 111949. 10.1016/j.corsci.2024.111949

Publishers page: <http://dx.doi.org/10.1016/j.corsci.2024.111949>

Please note:

Changes made as a result of publishing processes such as copy-editing, formatting and page numbers may not be reflected in this version. For the definitive version of this publication, please refer to the published source. You are advised to consult the publisher's version if you wish to cite this paper.

This version is being made available in accordance with publisher policies. See <http://orca.cf.ac.uk/policies.html> for usage policies. Copyright and moral rights for publications made available in ORCA are retained by the copyright holders.



1 **Molecular mechanism of the sulfide corrosion of α -iron**

2

3 J. B. Murowchick¹, A. Oldroyd² and D. Rickard²

4

5

6

7 ¹ Corresponding Author

8 Earth & Environmental Sciences, University of Missouri-Kansas City, Kansas City, MO, 64110,

9 USA

10 murowchickj@umkc.edu

11 ²School of Earth and Environmental Sciences, Cardiff University, Cardiff CF10 3AT, UK.

12 Oldroyd@cardiff.ac.uk

13 Rickard@cardiff.ac.uk

14

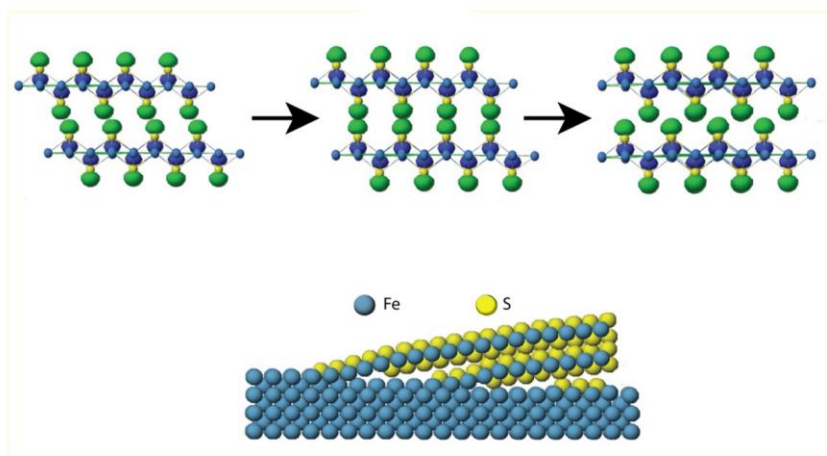
15

16 **Highlights**

- 17
- 18
- 19
- 20
- 21
- 22
- 23
- 24
- 25
- 26
- 27
- 28
- 29
- 30
- 31
- 32
- The reaction between aqueous sulfide and α -Fe is epitactic and the rate is dominated by the spallation of tetragonal FeS from the metal surface.
 - Spallation is caused by strains set up through the variations in the Fe-Fe distance in α -iron and the mackinawite structure.
 - Molecular modelling and simulated XRD spectra closely reproduce the experimental results confirming the process.

33 **Graphical abstract**

34



Commented [JM1]: Change S color, remove axes

38 **Abstract**

39 The reaction between aqueous sulfide and α -iron at ambient temperatures produces a ferrous
40 monosulfide with a tetragonal mackinawite structure, FeS_m . The reaction is epitactic with the Fe
41 structure in FeS_m being similar, but not identical, to the Fe structure in α -iron. The strain induced
42 by these small structural differences ultimately results in spallation of the FeS_m product. This
43 causes the exposure of new α -iron sites and determines the rate of sulfide corrosion of α -iron. The
44 results provide a fundamental explanation for the real-world observation that pitting of stainless
45 steel pipes in sulfide environments is a major source of corrosion and pipe failure.

46
47 X-ray diffraction analyses of the FeS_m product with time shows the development of anomalous
48 ratios of the intensities of the mackinawite (112) and (200) reflections and a complex change in the
49 length of the $d(100)$ interplanar spacing during FeS_m crystal growth on α -iron. Molecular
50 mechanics simulations and computed X-ray diffraction spectra demonstrate that these variations in
51 the FeS_m crystal structure with time are caused by movement of S-Fe-S layers of FeS_m to low
52 energy sites on the α -iron surface. The initially-formed S-Fe-S layers have relative positions
53 controlled by the arrangement of Fe atoms in the α -iron and are offset relative to the ideal
54 mackinawite structure. The computed relative intensities of the mackinawite (112) and (200) peaks
55 then change with time as the mackinawite S-Fe-S layers move from the α -iron position to the
56 mackinawite position. At the same time, each S $3p_z$ lone pair orbital in the mackinawite S-Fe-S
57 sheet projects toward a point equidistant from the four nearest lone pairs in the facing layer. The
58 lateral adjustment of the layers causes the interaction of S $3p_z$ lone pairs in adjacent layers to first
59 increase, then decrease during crystal growth. Repulsion between the layers consequently

60 increases, then decreases during crystal growth, with a resultant increase, then decrease in the
61 $d(001)$ spacing of the newly-formed FeS_m product.

62

63

64

65

66

67

68

69

70

71

72

73

74

75

76 **1 Introduction**

77 Mackinawite is the naturally-occurring tetragonal form of FeS, described originally by Evans Jr,
78 Milton, Chao, Adler, Mead, Ingram and Berner [1] and Kuovo, Vuorelainen and Long [2]. A
79 similar material was originally described as "kansite" [3] formed through the sulfide corrosion of
80 iron pipes. Berner [4] found it occurring on iron scrap in Mystic River, Connecticut, and defined
81 its tetragonal structure. We refer to any material with a composition approaching iron monosulfide
82 as FeS. We refer to synthetic FeS with a mackinawite structure as FeS_m and distinguish this from
83 the naturally-occurring mineral, mackinawite. A key to the abbreviations used in the text is shown
84 in Table 1.

85

86 **Table 1. Key to frequently used abbreviations herein, other abbreviations are defined in the**
87 **text.**

88

Abbreviation	Definition
α -Fe	α -iron
(hkl)	specific crystal plane
[hkl]	crystal direction
a, b, c	mackinawite tetragonal unit cell dimensions
$d(hkl)$	Interplanar spacing
FeS	iron monosulfide
FeS _m	synthetic mackinawite
I	X-ray diffraction intensity of a (hkl) reflection
mk	Mackinawite

89

90 FeS_m has been found to be an important corrosion product in the petroleum industry, sewage
91 transport/treatment environments, and the Girdler-sulfide process for making heavy water in the
92 nuclear industry [5].

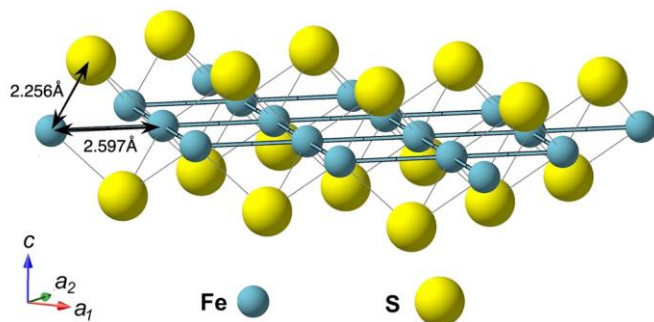
93

94 The composition of FeS_m was shown to be stoichiometric FeS [6]. The result confirmed the
95 conclusion of an earlier crystallochemical study [7] which reported no evidence for vacancies or
96 excesses in the mackinawite structure. Previous renderings of the composition as Fe-excess, Fe_{1+x}S
97 or Fe-deficient, Fe_{0.9}S, were shown to be due to analytic error. There is also a problem with the
98 facile partial cryptic transformation of mackinawite to greigite (Fe₃S₄) which may result in Fe:S
99 ratios deviating from unity [8]. Natural mackinawites associated with high temperature magmatic
100 sulfide ores often show extremely high (≤ 15 wt %) contents of other metals, including Ni, Co, Cu
101 and Cr. Indeed, mackinawite was the main Ni-bearing phase of the Hitura Ni deposit, Finland.
102 Analytic imprecision also led to the idea that the metal:sulfur ratios of these mackinawites varied
103 from unity.

104

105 The tetragonal structure of FeS_m was first reported by Berner [4]. Subsequently, the mackinawite
106 crystal structure (Figure 2) was described by [2], [9], [10] and [11] and finally refined by [7],
107 who reported that the cell parameters are $a=b=3.735 \text{ \AA}$ and $c = 5.0329 \text{ \AA}$.

108



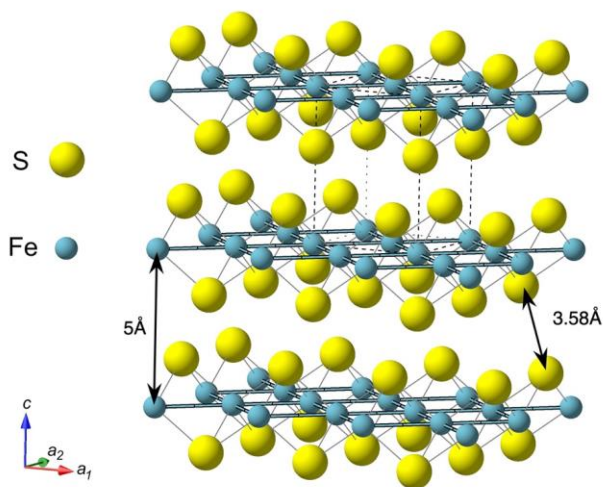
Commented [JM2]: Change colors—S yellow, Fe—blue-gray

109

110 **Figure 1. The basic structural unit of mackinawite consists of a square planar array of Fe**
 111 **atoms (Fe-Fe distance 2.597 Å) tetrahedrally coordinated with S atoms (Fe-S distance 2.256**
 112 **Å). A ball and stick view from 30° above the (001) plane emphasizing the extensive Fe-Fe**
 113 **bonding (from an original representation by [12])**

114

115 The basic structural unit of mackinawite is sheets of Fe atoms with perfect square planar
 116 coordination [7], tetrahedrally coordinated with S atoms (Figure 1). Delocalization of electrons in
 117 the Fe-Fe sheets was suggested as long ago as 1971 by [13] and strong Fe-Fe metallic bonding was
 118 confirmed by [7]. The Fe-Fe distance is 2.597, which is similar to the 2.866 Å Fe-Fe distance of α-
 119 iron.



Commented [JM3]: Change colors

120
 121 **Figure 2. Stacked FeS sheets in the c -direction (Figure 1) produce the mackinawite structure,**
 122 **with a tetragonal unit cell (dashed lines), 3.58 \AA between S atoms in adjacent sheets and the**
 123 **characteristic *ca.* 5 \AA (001) reflection caused by the vertical separation distance of the sheets**
 124 **(Ball and stick structural rendering form an original idea by [12]).**

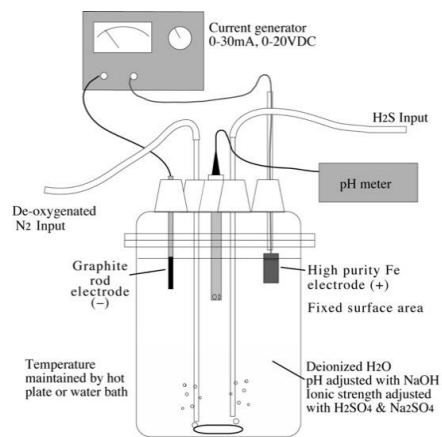
125
 126 The sheets are stacked normal to the c axis (Figure 2), and the stacked sheets are held together by
 127 weak van der Waals forces. The S atoms have a square pyramidal coordination with Fe and have a
 128 lone pair of electrons (primarily $3p_z$ character) projecting away from the plane of the sheet, toward
 129 a point equidistant from the four nearest (3.58 \AA) sulfur atoms in the overlying sheet. The result is
 130 an average distance between the sheets of approximately 5 \AA , which together with the shorter
 131 distance between the Fe atoms in the square planar array produces the characteristic tetrahedral
 132 symmetry of mackinawite.

133 **2 Methods**

134 **2.1 Experimental**

135 Mackinawite was synthesized for this study in a 1-L glass reaction vessel with five ports in the lid
136 for the anode and cathode, a pH electrode, and H₂S with deoxygenated N₂ inputs (Figure 3).

137



138

139 **Figure 3. Experimental apparatus.**

140 High-purity deionized water was sparged for 30 minutes with deoxygenated N₂ that was bubbled
141 through a pyrogallol solution (to eliminate the last traces of O₂) before entering the reaction vessel.
142 The sulfide concentration was controlled by either the PH₂S or by neutralizing a NaOH solution of
143 desired concentration. For runs above pH 7, in which HS⁻ was the dominant aqueous sulfide
144 species, NaOH was first added at a concentration equal to the desired HS⁻ concentration. H₂S was
145 then bubbled through the vessel until the desired pH was obtained. Below pH 7, where H₂S
146 becomes the dominant sulfide species (approximately 0.1m for saturation at 1 bar), the ionic

147 strength of the solution was adjusted to match that of the HS⁻ runs by the addition of Na₂SO₄ and
148 H₂SO₄, which also helped set the pH for the experiments. A cylindrical graphite electrode was
149 immersed through one of the ports, and the high purity iron plate was partially immersed in the
150 opposite port, approximately 10cm from the graphite electrode. The back and top of the front of
151 the plate were covered with paraffin so that the reactive area of the plate (2.25cm²) would remain
152 constant from run to run, and so that all of the product would be deposited on the front of the plate
153 where it is accessible for X-ray diffraction analysis *in situ*. The gold-plated alligator clip at the top
154 of the plate was kept out of the solution so that it did not become part of the electrode area. The
155 iron plate (cathode) and graphite (anode) were attached to a DC power supply that could produce 0
156 to 50mA current through the solution at about 0-20V potential. The current was set at 1mA to
157 30mA with the voltage increasing with current, and decreasing with increasing ionic strength at a
158 fixed current.

159 The current was manually controlled (± 0.05 to 0.5mA, depending on the experimental conditions),
160 and auxiliary resistors were sometimes added to the circuit at low currents to decrease the
161 sensitivity of the output to changes in the position of the controlling potentiometer. A pH
162 electrode was inserted in the fifth port, and the pH was measured at the beginning and end of each
163 run when the current generator was off and disconnected. Most runs were at ambient temperature,
164 20-22°C, but the vessel was placed in a constant temperature water bath for run temperatures to
165 45°C. The duration that current was applied was recorded as the run duration.

166 Upon completion of a run, the plate was taken out of the vessel and immediately immersed in
167 acetone. In the case of the low pH runs, a quick but gentle dip in water before the acetone
168 removed the Na₂SO₄ (which crystallized on the sample unless removed by the washing), without
169 disturbing the product. The sample was then removed from the acetone, quickly air-dried, and

Commented [SM4]: It is not clear what duration current means...

170 mounted in the X-ray diffractometer using the iron plate as the sample support. This method
171 permitted very small amounts of FeS_m to be detected on the iron surface while the α -iron acted as
172 an internal standard for 2 θ . A check using X-ray diffraction and SEM examination showed that
173 preferred orientation was not a problem, primarily because of the very small particle size and
174 multiple orientations of the Fe grains in the plate.
175 The FeS_m was removed from the plate with 1M hydrochloric acid, followed by a water rinse and
176 drying with acetone. The mass of the iron plate with and without the sulfide product was measured
177 with a Sartorius R 160 P precision microbalance with a sensitivity of 0.01 mg and a precision of \leq
178 0.02 mg. The mass of FeS_m produced was calculated from the mass difference between the plate
179 with FeS and the mass of the Fe plate after stripping off the FeS with HCl. A test using an
180 unreacted Fe plate showed that no measurable loss of mass of metallic Fe occurred during the
181 rapid HCl dip. The mass of reacted S was calculated from the mass difference between the plate
182 mass before reaction and the mass of the plate with FeS after each run.

183 2.2 Computational

184 The digitized X-ray diffractogram output was analyzed using both the built-in Philips APD
185 software, and MacDiff 3.2.4 PPC [14]. Calculated X-ray diffractograms of hypothetical
186 mackinawites with various amounts of interlayer offset were obtained using the Diffraction-Crystal
187 package of Cerius2 from Molecular Simulations, Inc. (Burlington, MA).
188

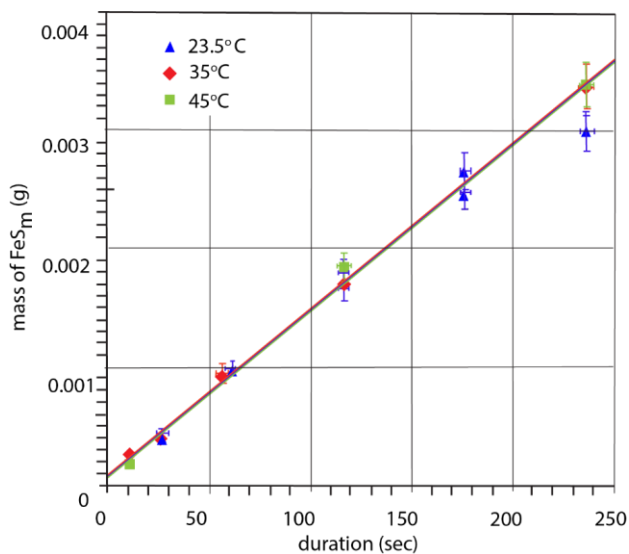
189 The extended-Hückel and molecular mechanics investigation of the bonding in mackinawite
190 utilized the Extended Hückel and Molecular Mechanics packages, respectively, of CAChe
191 Worksystem 3.6 (Oxford Molecular) for atomic and molecular orbital structures of fragments of
192 the mackinawite structure. YAeHMOP 2.0 and MacYAeHMOP 2.0b [15] were used to calculate
193 the band structure, density of state projections, and crystal orbital overlap populations for larger

194 portions of the mackinawite structure. Optimized K-point grids for the YAeHMOP calculations
195 were obtained using the method of Ramirez and Böhm [16, 17] with the program Kgrid.

196 3 Results

197 3.1 Experimental

198 The mass of synthetic mackinawite produced increased nearly linearly with the duration of
199 synthesis (Figure 4). The slight curvature of some plots with synthesis times longer than 50
200 minutes (not shown) is probably due to the spalling of material during a run, especially at high
201 currents, long run duration or high stirring rates. That is, the mass of FeS_m formed as measured by
202 the difference in weights between the coated iron plate and the HCl-stripped iron plate was
203 underestimated since, under these more extreme conditions, increasing fractions of the FeS_m
204 produced ended up in the reaction flask and not attached to the weighed plate.
205



206

207 **Figure 4. Mass of FeS_m(g) versus time (sec) for mackinawite syntheses at pH 8.1, 30.0mA,**
208 **2.1-2.5 V between 23.5 and 45°C. The estimated errors are shown for ± 5.5% mass and ±3 sec**
209 **duration. The amount of FeS_m increases with time almost linearly (R² = 0.993 to 0.996)**

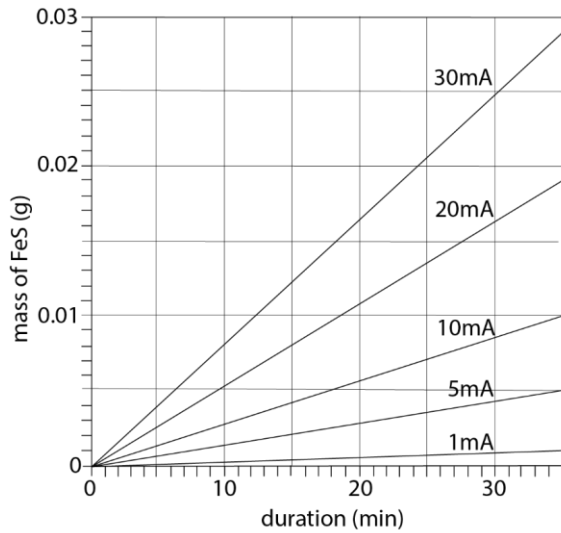
210 The precision of the results for the mass of FeS_m produced can be evaluated by comparing the
211 results with the theoretical mass of FeS produced (Figure 5). The equation for the formation of FeS
212 through the reaction of aqueous sulfide with α-Fe (1) results in the production of 2 electrons for
213 each mole of FeS formed.



215 These 2 electrons per mole of FeS are provided by the current, *I*, in amperes, imposed on the
216 electrode. The rate of production of electrons ($\text{e}^- \text{ s}^{-1}$) is given by Equation (2) where C (Coulombs)
217 is the total charge carried by 6.24×10^{18} electrons and *t* is the duration of the experimental run
218 (seconds).

219
$$\text{e}^- \text{ s}^{-1} = 6.25 \times 10^{18} I / t \quad (2)$$

220
221 Then from (1), the number of FeS molecules formed per unit time is $6.25 \times 10^{18} I / 2t$ and the mass of
222 FeS formed per unit time is simply obtained from Avogadro's number.
223



224
 225 **Figure 5. Calculated FeS production (g) versus experimental duration for current settings**
 226 **between 1 and 30mA for an Fe electrode surface area of 2.25cm².**

227
 228 The theoretical rate of FeS formation at 30mA current is $1.37 \times 10^{-5} \text{g s}^{-1}$. This is compared with
 229 observed values for the rate of FeS_m formation in Table . The computed rates compare closely with
 230 the observed rate providing a further confirmation of the accuracy of the measurement method.
 231 The observed rates in Figure 4 intersect the y-axis (FeS_m mass) at finite values (Table 1) which
 232 suggests that a mass of FeS (between 1.60 and $1.91 \times 10^{-4} \text{g}$) is formed within the first seconds of
 233 the reaction. The rate of precipitation of FeS_m from solution has been shown to be virtually
 234 instantaneous in geological terms (Rickard 1995) and to occur within a millisecond of the initiation
 235 of the reaction. This means that the rate of nucleation of mackinawite is extremely rapid, consistent
 236 with the observations of the present experimentation. The mass at times approaching 0 seconds

237 indicated in Table 2 and on Figure 5 reflects this initial nucleation-dominated stage. The results
238 show that the observed rate curves (e.g., Figure 4) record the subsequent growth of FeS_m crystals.
239

240

241 **Table 2. Comparison of measured rates of FeS_m production in terms of the slope of the**
242 **curves shown in Figure 3 for various temperatures (T°C) with the computed rate of FeS**
243 **formation. The intercept is the mass on the y-axis (g) for the computed R² values and reflects**
244 **the extremely rapid rate of FeS_m nucleation (see text).**

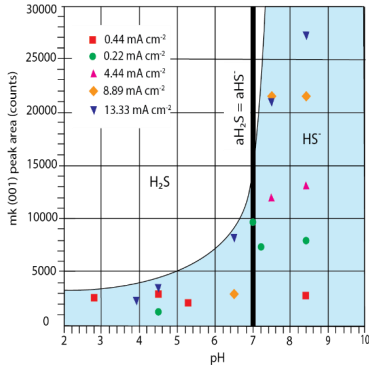
T (°C)	Rate (g s ⁻¹)	Intercept (g)	R ²
23.5	1.42 x 10 ⁻⁵ t	1.60 x 10 ⁻⁴	0.993
35	1.42 x 10 ⁻⁵ t	1.78 x 10 ⁻⁴	0.996
45	1.41 x 10 ⁻⁵ t	1.91 x 10 ⁻⁴	0.996
computed	1.37 x 10 ⁻⁵ t	0	

245

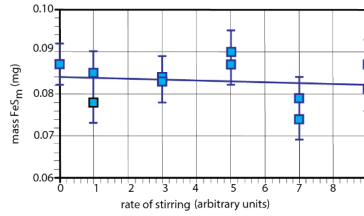
246

247 The rate of formation of synthetic mackinawite was strongly affected by pH. Above pH 7.0, FeS_m
248 formed rapidly and abundantly on the electrode. However, below pH 7.0, FeS_m formation was
249 very slow (Figure 6a). The pH was adjusted to pH 8 in most of the experiments so that efficient
250 FeS_m production was obtained, and so HS⁻ was the dominant reduced S species present.
251

252 The rate of stirring also had a negligible effect on the rate of FeS_m formation (Figure 6b), though at
253 the highest stirring rates (about 700rpm), flakes of product were more rapidly removed from the
254 electrode surface. The lack of any stirring rate dependence is consistent with the negligibly low
255 apparent activation energy and suggests that the reaction is not diffusion-controlled.
256



(a)



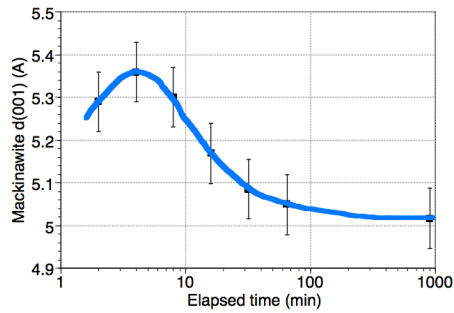
(b)

257
 258 **Figure 6. (a) Effect of pH on mackinawite synthesis. (b) Effect of stirring rate (arbitrary**
 259 **units) on the rate of mackinawite synthesis (pH 8.1, 20°C, 60 sec).**

260 The effect of temperature on the rate of synthetic mackinawite formation in the experiments (see
 261 Figure 4) was found to be negligible (20° to 45°C). However, the activation energy for the reaction
 262 at all three temperatures is likely exceeded by the applied voltage in the experiments, obscuring
 263 any temperature dependence of the reaction rates.

264 Two types of anomalies were noted in the X-ray diffractograms. Firstly, the mk $d(001)$ of the
 265 product increased (to as high as 5.35Å), then decreased to the normal mackinawite $d(001)$ of
 266 5.03Å with time during each synthesis (**Error! Reference source not found.**). With high current
 267 densities (20-30mA/2.25cm²), the maximum $d(001)$ occurred earlier in the run than when the
 268 current density was low (1-10mA/2.25cm²), but the same general behavior was observed over a
 269 range of current densities.

270



271

272 **Figure 7. Variation of d(001) during crystal growth of FeS_m.**

273

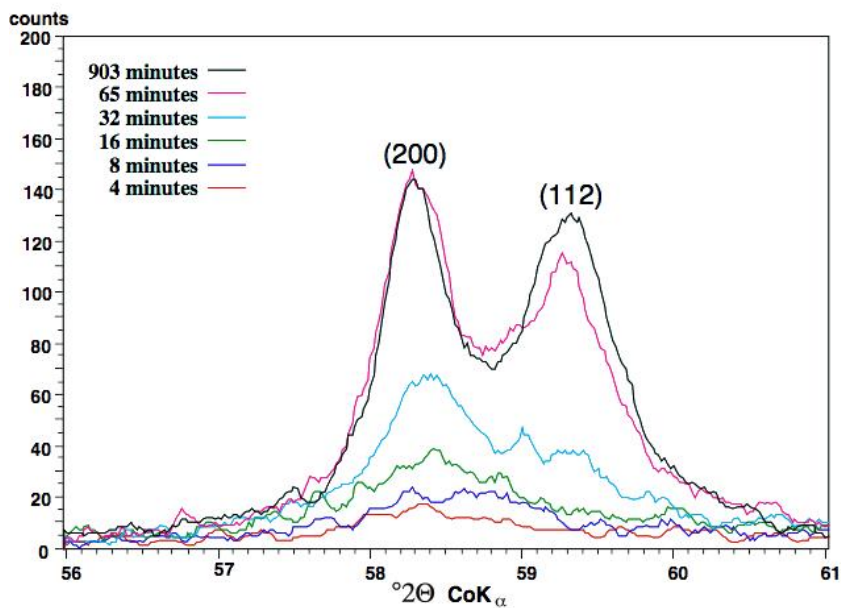
274 The second anomaly observed in the X-ray diffractograms was that the ratio of the (200) and (112)
 275 peak intensities varied greatly with time, with the (112) peak initially being weak to absent, then

276 rapidly increasing in intensity until it approached the normal intensity (Figure). Similar behavior

277 was observed for experiments using other currents. |

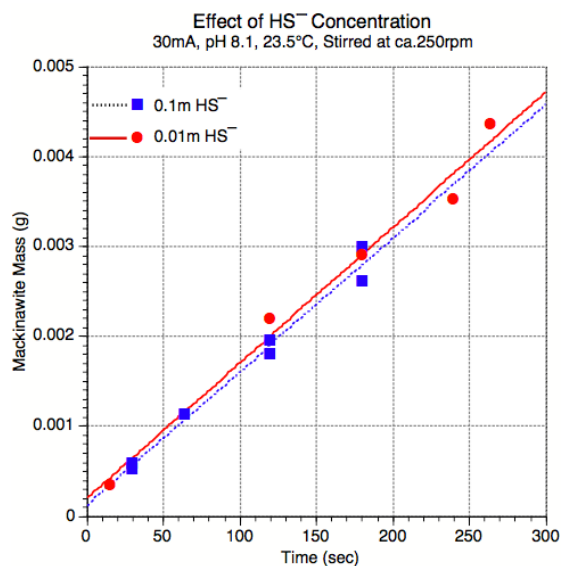
Commented [JM5]: Remove colored background.

278 |



279
 280 **Figure 8. Experimental X-ray diffractograms of the (200) and (112) peaks of synthetic**
 281 **mackinawite at various times between 4 and 903 minutes at 5mA current, pH 7.0 and 20°C**

282
 283 The effect of HS⁻ concentration on the reaction rate was negligible (Figure 9) for the range of HS⁻
 284 concentrations used in the experiments. Such behavior reflects the surface reaction control of the
 285 reaction rate as long as there is an excess of HS⁻ in the solution adjacent to the Fe plate.

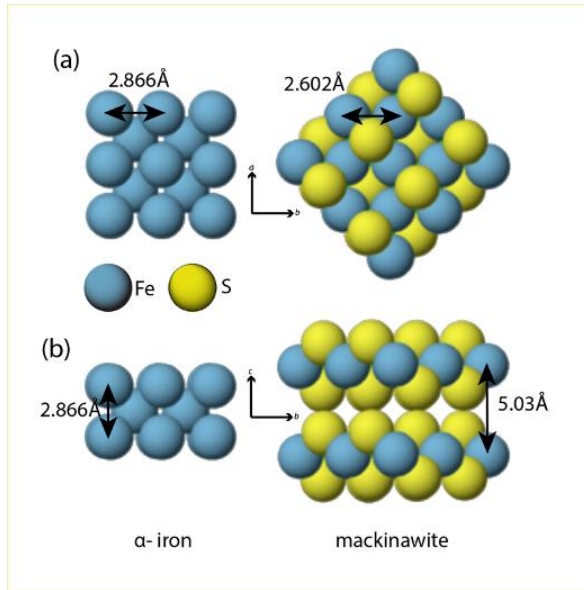


287 **Figure 9. FeS_m production vs time at different HS⁻ concentrations.**

288 **4 Discussion**

289 The arrangement of Fe atoms in mackinawite is similar to that in α -iron (Figure). The Fe-Fe
 290 distance in a (001) layer is 2.866Å, comparable to the corresponding Fe-Fe distance of 2.602Å in
 291 mackinawite. The insertion of S into the α -Fe structure results in the expansion in the distance
 292 between the Fe layers, resulting in the tetragonal symmetry of mackinawite.

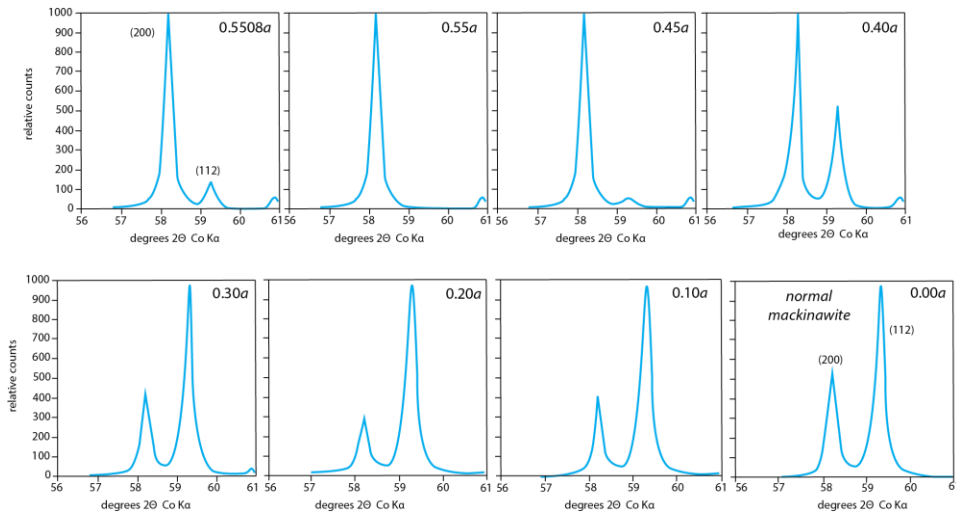
293



Commented [JM6]: Fix S color

294
 295 **Figure 10. Comparison of α -iron and mackinawite structures showing their intrinsic**
 296 **congruity: (a) plan view (looking down the c-axis) showing homology of α -iron and**
 297 **mackinawite structures; (b) cross-section (looking along the a-axis) showing the expansion of**
 298 **the Fe layers in the mackinawite structure.**

299
 300 The similarities of the mackinawite and α -iron structures (Figure) promote epitactic nucleation of
 301 mackinawite on α -iron. The Fe-Fe distance of 2.602Å along mk[110] or $[\bar{1}10]$ is comparable to
 302 the α -iron Fe-Fe distance of 2.866Å along [100], [010], or [001] of α -iron. In the mackinawite
 303 structure, the iron atoms in one S-Fe-S layer are directly below those in the overlying layer in
 304 contrast to α -iron where the Fe atoms in subjacent layers are offset by $0.5a_1 + 0.5a_2$ along [110].
 305 The epitactic development of the mackinawite structure from α -iron then requires an offset of
 306 $0.5508a$ in adjacent Fe-layers along mk[100] or [010] in the mackinawite structure.



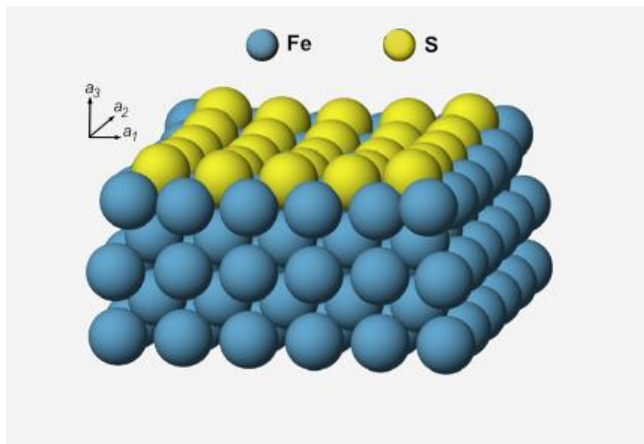
307

308 **Figure 11. Calculated X-ray diffractograms (relative counts versus 2θ , CoK α radiation) for**
 309 **the mackinawite structure in terms of relative offsets (in units of a , the size of the**
 310 **mackinawite unit cell in the a direction).**

311

312 Selected calculated X-ray diffractograms for the (200) and (112) reflections of mackinawite-like
 313 structures with various amounts of stacking offset of the (001) layers, from an offset of $0.5508a$ (a
 314 is the mackinawite unit cell dimension in the [100] direction) through to $0.00a$, are shown in
 315 **Figure 1**. The initial offset of $0.5508a$ is determined by the positions of the Fe atoms in adjacent
 316 layers in α -iron (Figure 10). Progressive slippage of layers along mackinawite [100] result in the
 317 subsequent diffractograms, culminating with the diffractogram for normal mackinawite ($0.00a$
 318 offset.

319

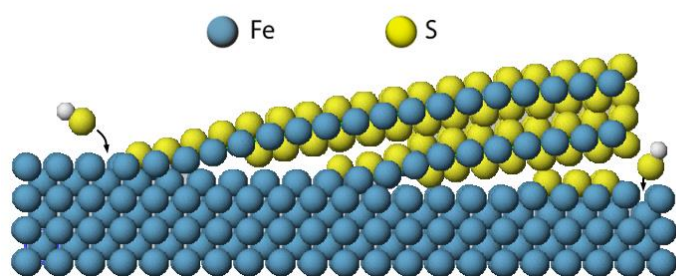


320
 321 **Figure 12. Molecular mechanics simulation of S adsorption on α -iron. The situation of sulfur**
 322 **atoms on the Fe surface is similar to elements of the mackinawite structure with the**
 323 **development of a noticeable curvature in the atomic pattern due to imposed contraction of**
 324 **the Fe-Fe distance in the near-surface Fe layer.**

325
 326 A molecular mechanics simulation of sulfur bonded to α -iron surface (Figure 2) shows that the
 327 strain introduced by the contraction of the near-surface Fe layers leads to curling of the S-Fe layer.
 328 Over a distance of several unit cells the strained area eventually detaches along one margin to
 329 relieve the accumulated stresses. The S-Fe layer then peels up and away from the underlying α -
 330 iron surface, exposing new sites for S adsorption on both the underside of the separating flake
 331 which acts to both counteract the curl and produce the complete S-Fe-S layer. At the same time the

332 underlying α -iron surface is exposed to further S-attack. As the process continues and is repeated,
333 underlying α -iron layers are exposed and a stack of S-Fe-S layers is formed (Figure 3).

334



335

336

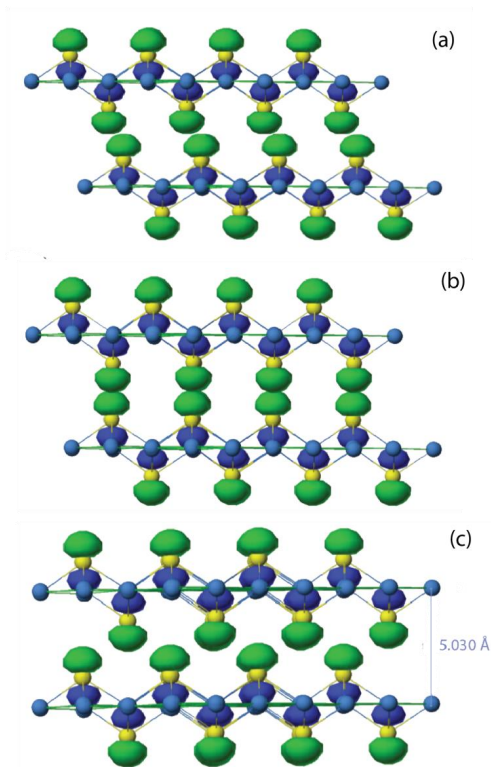
337 **Figure 13. Molecular mechanics simulation of synthetic mackinawite formation on α -iron.**

338 **Continued reaction of S (HS^- here) with surface Fe on α -iron leads to underplating and**
339 **detachment of FeS layers with further S leading to spalling of resultant FeS_m layers.**

340 Because alternate layers of Fe atoms in α -iron are offset, the resulting mackinawite-like S-
341 Fe-S layers will also be offset as long as the flakes are attached along one edge to the α -iron
342 structure. Complete detachment of the flake from the α -iron, or a change in the angle of
343 inclination of the flakes to the iron structure, permits lateral shifting of the layers (equivalent to
344 movement along $\text{mk}[100](001)$) by approximately $0.5a(\text{mk})$ to form a more mackinawite-like
345 structure during crystal growth.

346

Commented [JM7]: Change S color, remove xl axes



347

348

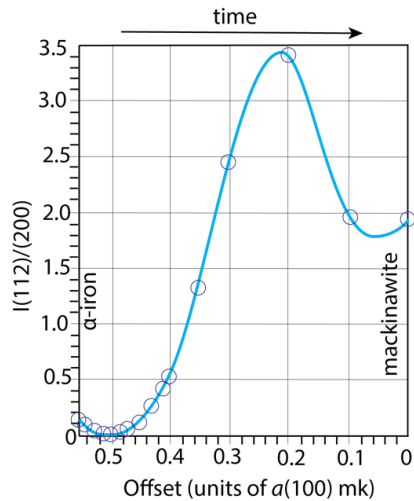
349 **Figure 14. Effect of S $3p_z$ non-bonding lone-pair orbitals on the development of the**
 350 **mackinawite structure: (a) Initial stage of formation; (b) at $0.5a$ offset (maximum**
 351 **repulsion); (c) normal mackinawite structure. The upward-pointing $3p_z$ lobes are offset into**
 352 **the page by $1/2a$ relative to the downward-pointing lobes.**

353

354 As long as the S-Fe-S layers are still attached to the α -iron structure, they are offset from one
355 another by the equivalent of about $0.5508a$ along $mk[100]$ or $[010]$. Non-bonding crystal orbitals,
356 dominantly S $3p_z$ in character and containing a lone pair of electrons, project from one S-Fe-S
357 layer toward the subjacent later. In the initial stage of formation (Figure 4a), the $mk(001)$ layers
358 are offset, bringing the S $3p_z$ lone pairs of one layer into close proximity with and between the lone
359 pairs of the facing layer. When the stacking offset is $0.5a$ (Figure 4c), the orbital lobes project
360 between two nearest S $3p_z$ lobes of the underlying layer. Extended Hückel density of states and
361 Fermi energy calculations using MacY AeHMOP (Landrum, 1996) indicate that at an offset of
362 $0.5a$, the Fermi energy is at a local maximum. Offsets greater than or less than $0.5a$ along
363 mackinawite $[100]$ or $[010]$ directions will be more stable, with the Fermi energy of the normal
364 mackinawite configuration (no offset) being at a minimum.

365 The continued tethering of the forming flakes to the α -iron structure causes the stacked S-Fe-S
366 layers to be dragged over the high-energy position before reaching the more stable mackinawite
367 arrangement (Figure 4c). Shifting of adjacent layers along $mk[100]$ by slightly more than $0.5a$
368 produces the normal mackinawite structure. Each S $3p_z$ lone pair orbital projects toward a point
369 equidistant from the four nearest lone pairs in the facing layer. The lateral adjustment of the layers
370 therefore requires that the interaction of S $3p_z$ lone pairs in adjacent layers first increase, then
371 decrease during crystal growth. Repulsion between the layers consequently increases, then
372 decreases during crystal growth, with a resultant increase, then decrease in the $d(001)$ spacing of
373 the newly-formed FeS_m product (**Error! Reference source not found.**).

374



375
 376 **Figure 15. Computed intensity ratios of the mackinawite (112) and (200) reflections (I**
 377 **(112)/(200)) versus offset of the Fe layers in units of fractions of the a (100) length in**
 378 **mackinawite showing effect of crystal growth of mackinawite from α -iron (offset 0.5508 a) to**
 379 **mackinawite (0 a).**

380
 381 Normal mackinawite is tetragonal (P4nm), giving the (200) XRD reflection a multiplicity of 4
 382 and the (112) reflection a multiplicity of 8. For these two reflections, multiplicity plays a major
 383 role in determining their relative intensities. If adjacent layers are offset along [100], the
 384 multiplicity of the (200) reflection drops to 2, but the multiplicity of the (112) reflection drops to 0,
 385 *i.e.*, the reflection is extinguished. If the initially-formed S-Fe-S layers have relative positions
 386 controlled by the arrangement of Fe atoms in the α -iron, the layers will be offset by 0.5508 a in

387 terms of the mackinawite structure. The computed relative intensities of the mackinawite (112)
388 and (200) peaks will then change with time as the mackinawite S-Fe-S layers move from the α -iron
389 position (at an offset of $0.5508a$ in the mackinawite structure) to the mackinawite position (at $0.0a$)
390 (Figure 5).

391
392 The intensity of the (001) reflection is not greatly affected by such a lateral shift. The major effect
393 on $d(001)$ is its change in size as the mackinawite structure develops. The distance between the S-
394 Fe-S sheets varies as they are dragged across the underlying sheets due to the repulsive effects of
395 the S $3p_z$ non-bonding lone-pair orbitals (Figure 4) producing the complex curve for mk $d(100)$
396 shown in **Error! Reference source not found.** The growth process thus explains the observed
397 anomalous X-ray diffraction reflections behavior of both the (001) peak (**Error! Reference source**
398 **not found.**) and the (200)/(112) behavior shown in Figure , 11, and 15.

399

400 5 Conclusions

401 Our experimental results demonstrate a mechanism for corrosion product layer growth in sulfide
402 corrosion which involves the epitactic growth of synthetic mackinawite and its subsequent
403 spallation due to strains caused by small deviations in the Fe-Fe distances in the mackinawite and
404 α -iron structures. The rapid formation of well-crystallized FeS_m , the negligible activation energy
405 for the reaction, and the anomalous behavior of both $d(001)$ and the intensities of the (112) and
406 (200) X-ray reflections all evidence the proposed mechanism.

407 Accumulated strain produced by contraction of Fe-Fe distances when S attaches to the Fe surface
408 leads to curling of the S-Fe layer away from the bulk iron and development of offset mackinawite-
409 like S-Fe-S layers. The intensities of the mk (112) and (200) reflections vary because of the

410 stacking adjustments of the S-Fe-S layers during crystal growth. Once an S-Fe-S layer is
411 disconnected from the α -Fe structure during crystal growth, adjacent S-Fe-S layers in FeS_m slide
412 from their offset positions toward commensurate positions. During that process, S $3p_z$ non-bonding
413 orbitals of one layer are temporarily brought into close proximity with those of the underlying
414 layer, causing increased interlayer repulsion and expansion of the interlayer spacing, $mk\ d(001)$.
415 Continued migration of layers along $mk[100]$ eventually bring the layers into the lower-energy
416 relationship found in mackinawite.

417 The experimental and computed results are consistent with a surface reaction, rather than a
418 purely aqueous reaction. The experimental results reveal that the dominant control of the rate of
419 the reaction under the conditions of our experiments is the mechanical process of exposing new
420 reactive sites on the α -iron surface as S-Fe-S layers are peeled away. This may provide support,
421 and a basic mechanism, for the real world observations that pitting of steel pipes in sulfide
422 environments is a major source of corrosion and pipe failure [e.g. 18, 19, 20].

423

424

425

426 **CRedit authorship contribution statement**

427 **James Murowchick:** Validation, Formal analysis, Investigation, Visualization, Data curation,
428 Methodology, Resources, Writing – original draft, Writing – review & editing. **Anthony Oldroyd:**
429 Methodology. **David Rickard:** Conceptualization, Writing, Supervision, Project administration,
430 Funding acquisition
431

432 **Declaration of Competing Interest**

433 The authors declare that they have no known competing financial interests or personal
434 relationships that could have appeared to influence the work reported in this paper
435

436

437 **Acknowledgements**

438 We thank Professor M. B. Hursthouse for his contribution to the XRPD work and its interpretation.
439 DR and AO acknowledge NERC grants GR9/603 and GR3/7476 and the EPSRC National
440 Service for X-ray Crystallography.
441

442 **Data Availability**

443 Data will be made available on request.

Figure Captions

Figure 1. The basic structural unit of mackinawite consists of a square planar array of Fe atoms (Fe-Fe distance 2.597 Å) tetrahedrally coordinated with S atoms (Fe-S distance 2.256 Å). A ball and stick view from 300 above the (001) plane emphasizing the extensive Fe-Fe bonding (from an original representation by [12])

Figure 2. Stacked FeS sheets in the c-direction (Figure 1) produce the mackinawite structure, with a tetragonal unit cell (dashed lines), 3.58 Å between S atoms in adjacent sheets and the characteristic ca. 5 Å (001) reflection caused by the vertical separation distance of the sheets (Ball and stick structural rendering from an original idea by [12]).

Figure 3. Experimental apparatus.

Figure 4. Mass of FeS_m(g) versus time (sec) for mackinawite syntheses at pH 8.1, 30.0mA, 2.1-2.5 V between 23.5 and 45oC. The estimated errors are shown for ± 5.5% mass and ±3 sec duration.

The amount of FeS_m increases with time almost linearly (R² = 0.993 to 0.996)

Figure 5. Calculated FeS production (g) versus experimental duration for current settings between 1 and 30mA for an Fe electrode surface area of 2.25cm².

Figure 6. (a) Effect of pH on mackinawite synthesis. (b) Effect of stirring rate (arbitrary units) on the rate of mackinawite synthesis (pH 8.1, 20oC, 60 sec).

Figure 7. Variation of d(001) during crystal growth of FeS_m in the experiments.

Figure 8. Experimental X-ray diffractograms of the (200) and (112) peaks of synthetic mackinawite at various times between 4 and 903 minutes at 5mA current, pH 7.0 and 20oC.

Figure 9. FeS_m production vs. time at different HS⁻ concentrations.

Figure 10. Comparison of α-iron and mackinawite structures showing their intrinsic congruity: (a) plan view (looking down the c-axis) showing homology of α-iron and mackinawite structures; (b)

cross-section (looking along the a-axis) showing the expansion of the Fe layers in the mackinawite structure.

Figure 11. Calculated X-ray diffractograms (relative counts versus 2θ , $\text{CoK}\alpha$ radiation) for the mackinawite structure in terms of relative offsets (in units of a , *the* size of the mackinawite unit cell in the a direction)

Figure 12. Molecular mechanics simulation of S adsorption on α -iron. The situation of sulfur atoms on the Fe surface is similar to elements of the mackinawite structure with the development of a noticeable curvature in the atomic pattern due to imposed contraction of the Fe-Fe distance in the near-surface Fe layer.

Figure 13. Molecular mechanics simulation of synthetic mackinawite formation on α -iron. Continued reaction of S (HS^- here) with surface Fe on α -iron leads to underplating and detachment of FeS layers with further S leading to spalling of resultant FeS_m layers

Figure 14. Effect of S 3pz non-bonding lone-pair orbitals on the development of the mackinawite structure: (a) Initial stage of formation; (b) at $0.5a$ offset (maximum repulsion); (c) **normal mackinawite structure**.

Figure 15. Computed intensity ratios of the mackinawite (112) and (200) reflections ($I(112)/(200)$) versus offset of the Fe layers in units of fractions of the a (100) length in mackinawite showing effect of crystal growth of mackinawite from α -iron (offset $0.5508a$) to mackinawite ($0a$).

References

- [1] H.T. Evans Jr, C. Milton, E.C.T. Chao, I. Adler, C. Mead, B. Ingram, R.A. Berner, Vallerite and the new iron sulfide, mackinawite, USGS Professional Paper 475-D, 475 D (1964) 64-69.
- [2] O. Kuovo, Y. Vuorelainen, J.V.P. Long, A tetragonal iron sulfide, American Mineralogist, 48 (1963) 511-524.
- [3] F.H. Meyer, O.L. Riggs, R.L. McGlasson, J.D. Sudbury, Corrosion products of mild steel in hydrogen sulfide environments, Corrosion, 14 (1958) 109-115.
- [4] R.A. Berner, Tetragonal iron sulfide, Science, 137 (1962) 669-670.
- [5] D.W. Shoesmith, P. Taylor, M.G. Bailey, D.G. Owen, The formation of ferrous monosulfide polymorphs during the corrosion of iron by aqueous hydrogen-sulfide at 21°C, Journal of the Electrochemical Society, 127 (1980) 1007-1015.
- [6] D. Rickard, A. Griffith, A. Oldroyd, I.B. Butler, E. Lopez-Capel, D.A.C. Manning, D.C. Apperley, The composition of nanoparticulate mackinawite, tetragonal iron(II) monosulfide, Chemical Geology, 235 (2006) 286-298.
- [7] A.R. Lennie, S.A.T. Redfern, P.F. Schofield, D.J. Vaughan, Synthesis and Rietveld crystal structure refinement of mackinawite, tetragonal FeS, Mineralogical Magazine, 59 (1995) 677-683.
- [8] D. Rickard, G.W. Luther, Chemistry of iron sulfides, Chemical Reviews, 107 (2007) 514-562.
- [9] E.F. Bertaut, P. Burlet, J. Chappert, Regarding the Absence of Magnetic Order in Quadratic Forms of FeS, Solid State Communications, 3 (1965) 335-338.
- [10] M. Uda, Structure of tetragonal FeS., Zeitschrift Fur Anorganische Und Allgemeine Chemie, 361 (1968) 94-98.
- [11] P. Taylor, L.W. Finger, Structural refinement and composition of mackinawite. , Carnegie Inst. Washington Yearbook, 69 (1971) 318-322.

- [12] M. Wolthers, S.J. Van der Gaast, D. Rickard, The structure of disordered mackinawite, *American Mineralogist*, 88 (2003) 2007-2015.
- [13] D.J. Vaughan, M.S. Ridout, Mössbauer studies of some sulphide minerals, *Journal of Inorganic and Nuclear Chemistry*, 33 (1971) 741-746.
- [14] R. Petschick, MacDiff 3.2.4 PPC. A tool for scientific graphical analysis of X-ray diffraction patterns. , in, Geologische-Paleontologisches Institut, Johann Wolfgang Goethe-Universitaet Frankfurt a.M., Germany, 1997.
- [15] G. Landrum, Yet another extended-Hückel molecular orbital package. (YAeHMOP and MacYAeHMOP, in, Cornell University New York, NY., 1996-7.
- [16] R. Ramirez, M.C. Böhm, Simple geometric generation of special points in Brillouin-zone integrations. Two-dimensional Bravais lattices, *International Journal of Quantum Chemistry* 30 (1986) 391-411.
- [17] R. Ramirez, M.C. Böhm, The use of symmetry in reciprocal space integrations. Asymmetric units and weighting factors for numerical integration procedures in any crystal symmetry, *International Journal of Quantum Chemistry*, 34 (1988) 571-594.
- [18] W. Zhang, B. Brown, D. Young, G. Bota, S. Nestic, M. Singer, Pitting mechanism of mild steel in marginally sour environments-Part I: A parametric study based on formation of protective layers, *Corrosion Science*, 183 (2021).
- [19] W. Zhang, B. Brown, D. Young, M. Singer, Pitting mechanism of mild steel in marginally sour environments ? Part II: Pit initiation based on the oxidation of the chemisorbed iron sulfide layers, *Corrosion Science*, 184 (2021).

[20] W. Zhang, B. Brown, D. Young, S. Smith, S. Huizinga, M. Singer, Pitting Mechanism of Mild Steel in Marginally Sour Environments: Pit Propagation Based on Acidification by Catalytic Oxidation of Dissolved Hydrogen Sulfide, *Corrosion*, 78 (2022) 142-151.

Tables

Table 2. Key to frequently used abbreviations herein, other abbreviations are defined in the text.

Abbreviation	Definition
α -Fe	α -iron
(hkl)	specific crystal plane
[hkl]	crystal direction
a, b, c	mackinawite tetragonal unit cell dimensions
$d(hkl)$	Interplanar spacing
FeS	iron monosulfide
FeS _m	synthetic mackinawite
I	X-ray diffraction intensity of a (hkl) reflection
mk	Mackinawite

Table 2. Comparison of measured rates of FeS_m production in terms of the slope of the curves shown in Figure 3 for various temperatures (T°C) with the computed rate of FeS formation. The intercept is the mass on the y-axis (g) for the computed R² values and reflects the extremely rapid rate of FeS_m nucleation (see text).

T (°C)	Rate (g s ⁻¹)	Intercept (g)	R ²
23.5	$1.42 \times 10^{-5}t$	1.60×10^{-4}	0.993
35	$1.42 \times 10^{-5}t$	1.78×10^{-4}	0.996
45	$1.41 \times 10^{-5}t$	1.91×10^{-4}	0.996
computed	$1.37 \times 10^{-5}t$	0	

Figure captions

Figure 7. The basic structural unit of mackinawite consists of a square planar array of Fe atoms (Fe-Fe distance 2.597 Å) tetrahedrally coordinated with S atoms (Fe-S distance 2.256 Å). A ball and stick view from 30° above the (001) plane emphasizing the extensive Fe-Fe bonding (from an original representation by [12])

Figure 8. Stacked FeS sheets in the c-direction (Figure 1) produce the mackinawite structure, with a tetragonal unit cell (dashed lines), 3.58 Å between S atoms in adjacent sheets and the characteristic ca. 5 Å (001) reflection caused by the vertical separation distance of the sheets (Ball and stick structural rendering form an original idea by [12]).

Figure 9. Experimental apparatus.

Figure 10. Mass of FeS_m(g) versus time (sec) for mackinawite syntheses at pH 8.1, 30.0mA, 2.1-2.5 V between 23.5 and 45°C. The estimated errors are shown for ± 5.5% mass and ±3 sec duration. The amount of FeS_m increases with time almost linearly ($R^2 = 0.993$ to 0.996).

Figure 11. Calculated FeS production (g) versus experimental duration for current settings between 1 and 30mA for an Fe electrode surface area of 2.25cm².

Figure 12. (a) Effect of pH on mackinawite synthesis. (b) Effect of stirring rate (arbitrary units) on the rate of mackinawite synthesis (pH 8.1, 20°C, 60 sec).

Figure 7. Variation of d(001) during crystal growth of FeS_m.

Figure 8. Experimental X-ray diffractograms of the (200) and (112) peaks of synthetic mackinawite at various times between 4 and 903 minutes at 5mA current, pH 7.0 and 20°C.

Figure 9. FeS_m production vs time at different HS⁻ concentrations.

Figure 10. Comparison of α -iron and mackinawite structures showing their intrinsic congruity: (a) plan view (looking down the c -axis) showing homology of α -iron and mackinawite structures; (b) cross-section (looking along the a -axis) showing the expansion of the Fe layers in the mackinawite structure.

Figure 11. Calculated X-ray diffractograms (relative counts versus 2θ , $\text{CoK}\alpha$ radiation) for the mackinawite structure in terms of relative offsets (in units of a , the size of the mackinawite unit cell in the a direction).

Figure 12. Molecular mechanics simulation of S adsorption on α -iron. The situation of sulfur atoms on the Fe surface is similar to elements of the mackinawite structure with the development of a noticeable curvature in the atomic pattern due to imposed contraction of the Fe-Fe distance in the near-surface Fe layer.

Figure 13. Molecular mechanics simulation of synthetic mackinawite formation on α -iron. Continued reaction of S (HS^- here) with surface Fe on α -iron leads to underplating and detachment of FeS layers with further S leading to spalling of resultant FeS_m layers.

Figure 14. Effect of S $3p_z$ non-bonding lone-pair orbitals on the development of the mackinawite structure: (a) Initial stage of formation; (b) at $0.5a$ offset (maximum repulsion); (c) normal mackinawite structure. The upward-pointing $3p_z$ lobes are offset into the page by $1/2a$ relative to the downward-pointing lobes.

Figure 15. Computed intensity ratios of the mackinawite (112) and (200) reflections ($I(112)/(200)$) versus offset of the Fe layers in units of fractions of the a (100) length in mackinawite showing effect of crystal growth of mackinawite from α -iron (offset $0.5508a$) to mackinawite ($0a$).

Figure 1

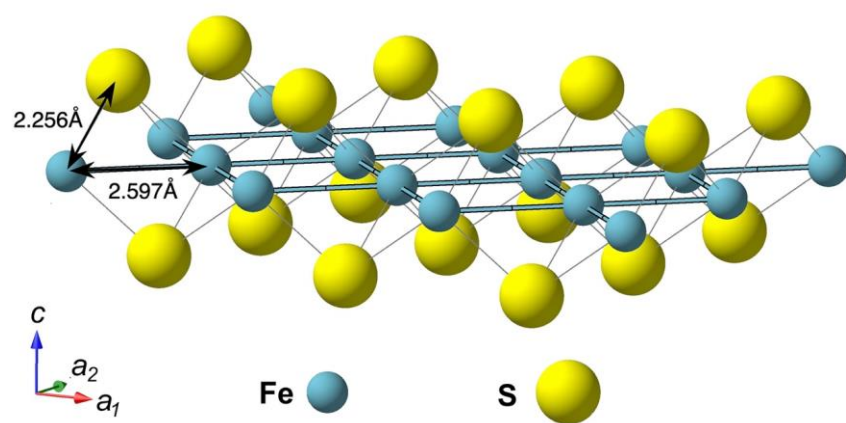


Figure 2

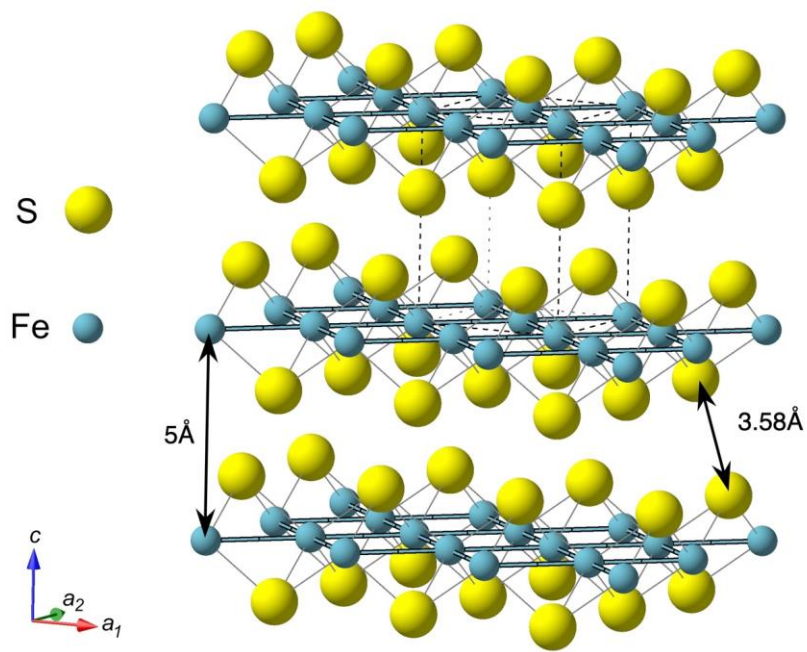


Figure 3

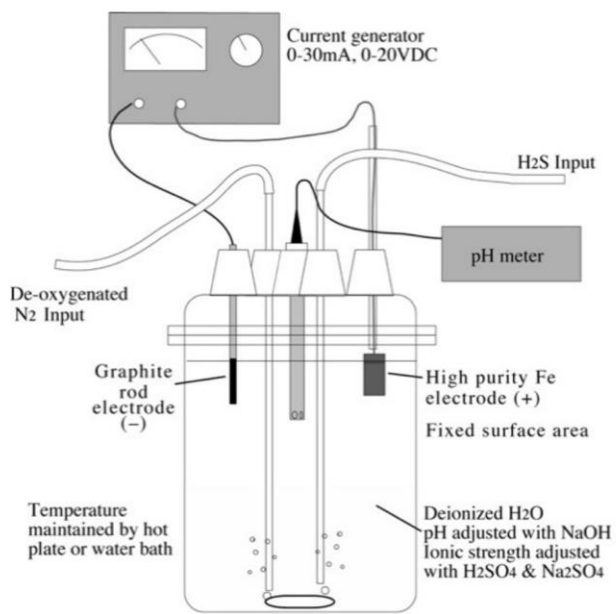


Figure 4

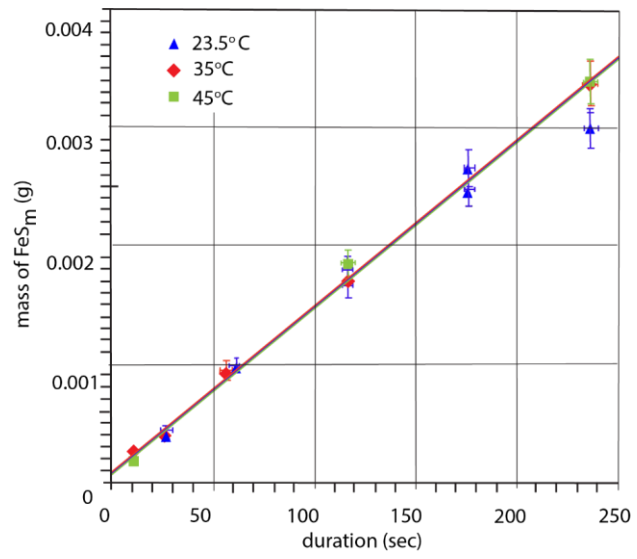


Figure 5

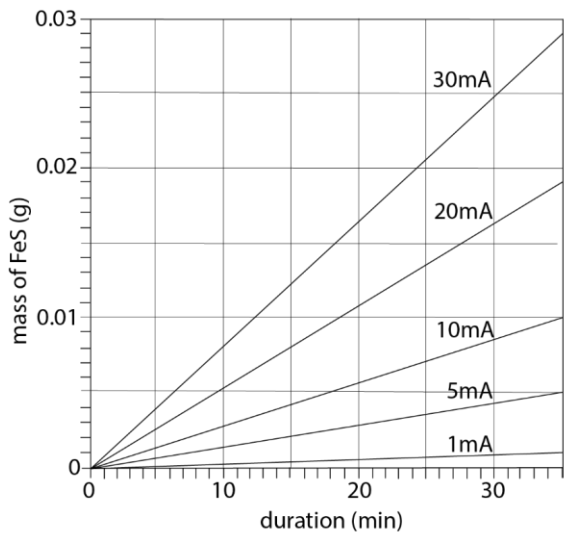
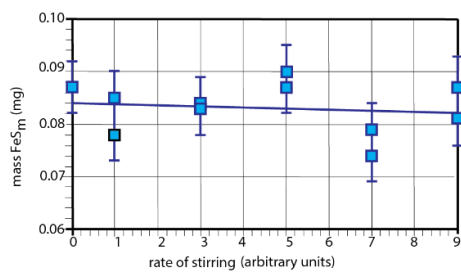
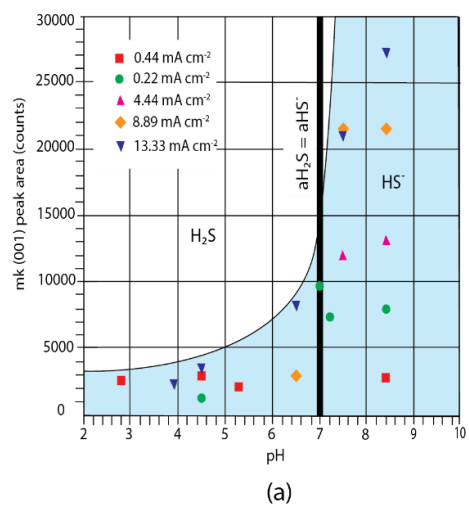


Figure 6



(b)

Figure 7

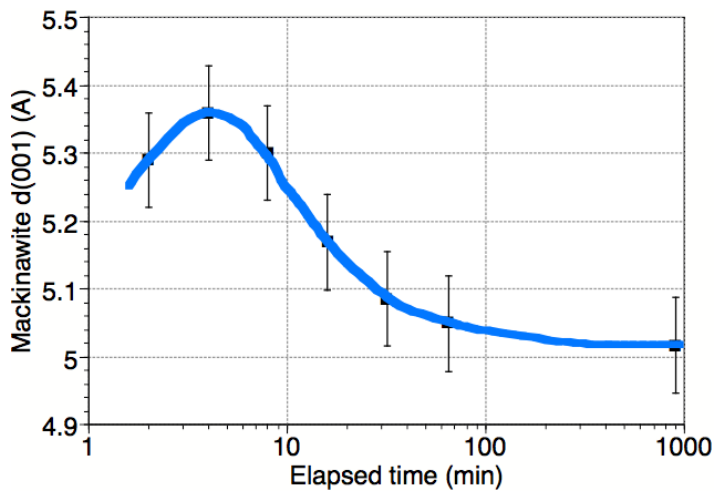


Figure 8

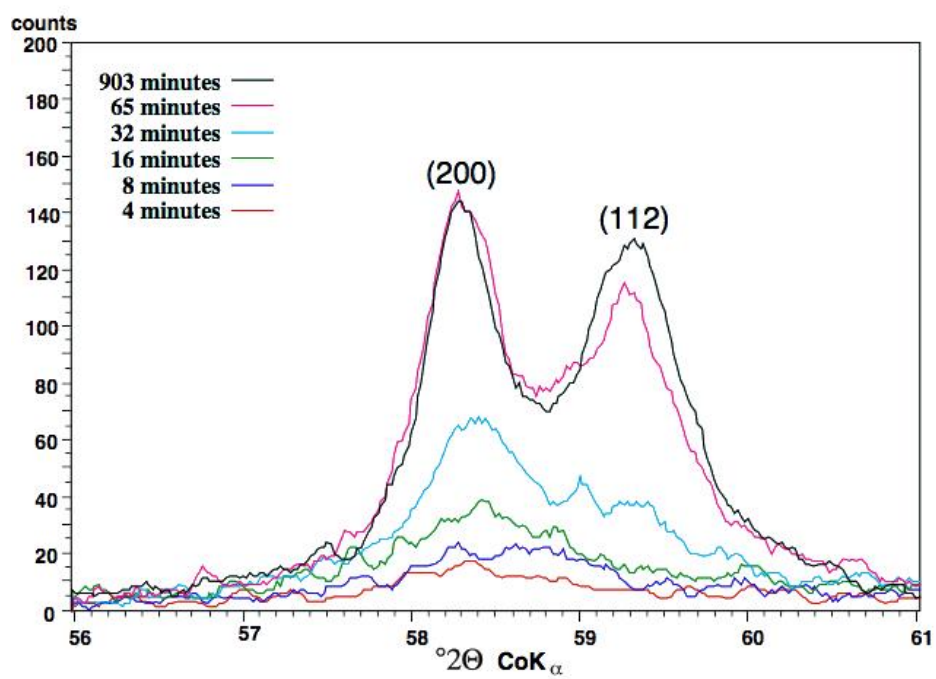


Figure 9

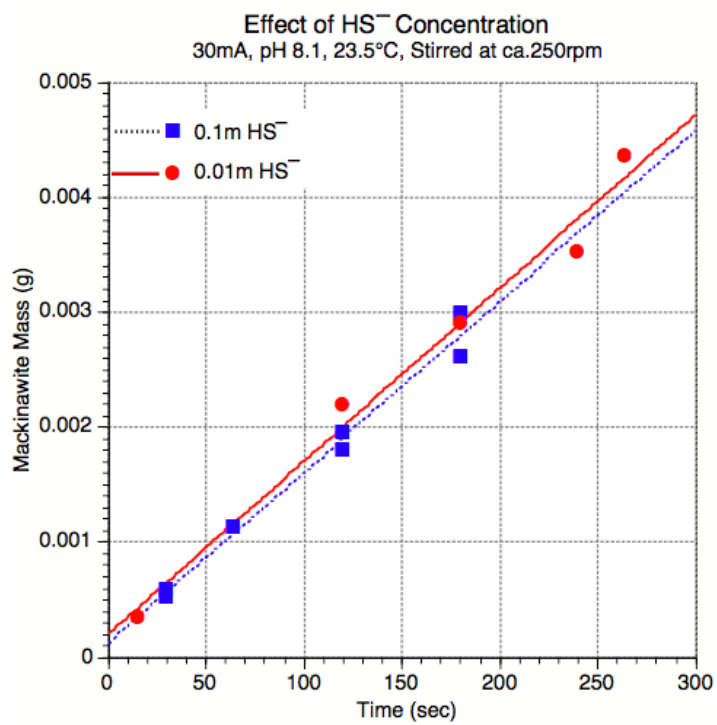


Figure 10

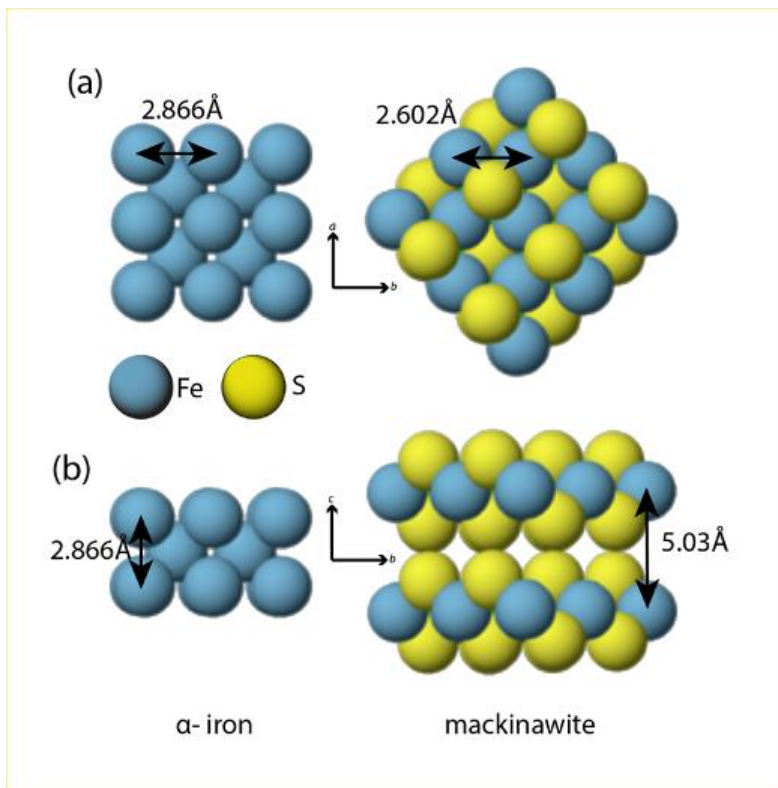


Figure 11

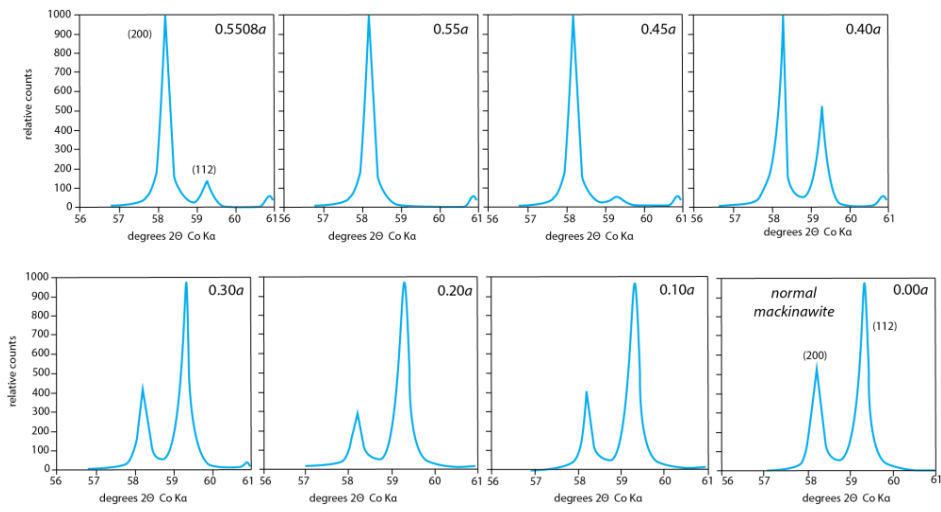


Figure 12

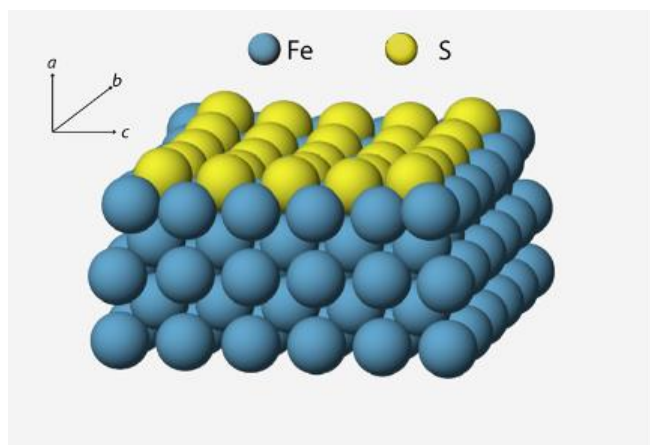


Figure 13

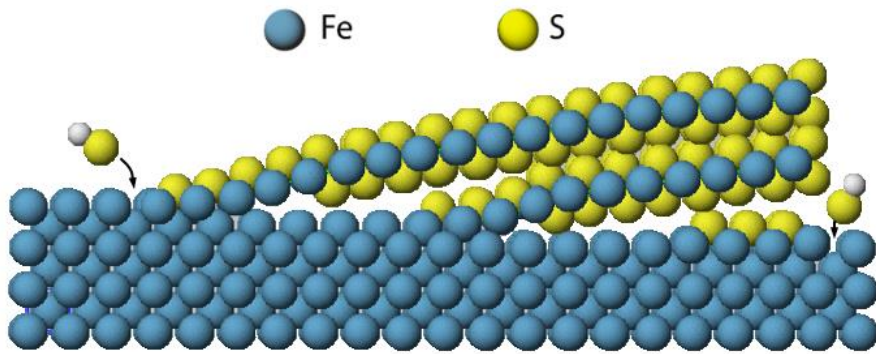


Figure 14

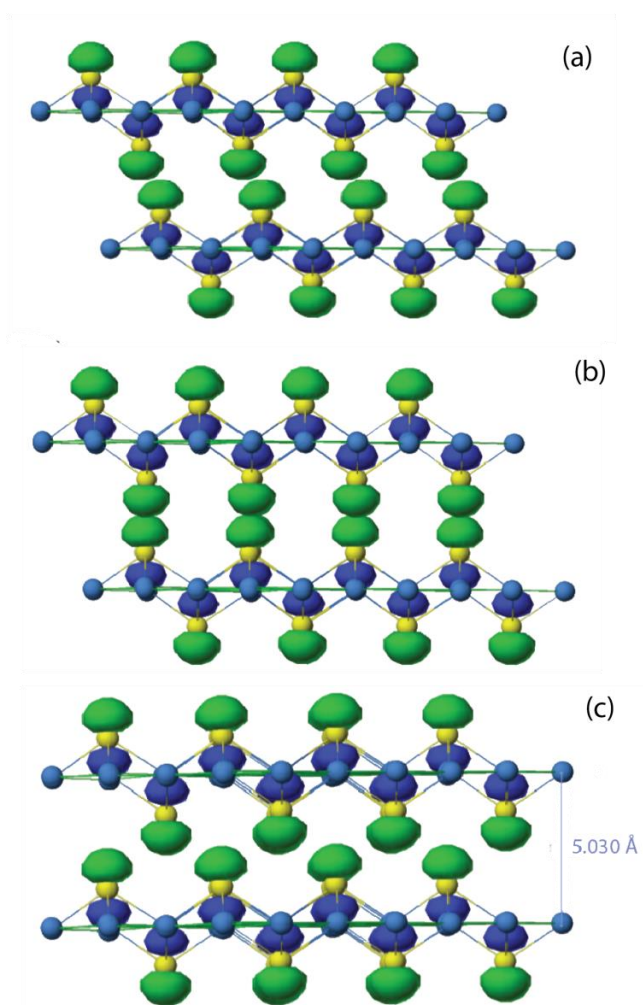


Figure 15

